Dissociations between glucose metabolism and blood oxygenation in the human default mode network revealed by simultaneous PET-fMRI

Lars Jonasson Stiernman[a,b,1], Filip Grill[b,c], Andreas Hahn[d], Lucas Rischka[d], Rupert Lanzenberger[d], Vania Panes Lundmark[a,b,c], Katrine Riklund[b,c], Jan Axelsson[b,c], and Anna Rieckmann[a,b,c,e,1]

[a]Department of Integrative Medical Biology, Umeå University, 90187 Umeå, Sweden; [b]Umeå Center for Functional Brain Imaging, Umeå University, 90187 Umeå, Sweden; [c]Department of Radiation Sciences, Umeå University, 90187 Umeå, Sweden; [d]Department of Psychiatry and Psychotherapy, Medical University of Vienna, 1090 Vienna, Austria; and [e]The Munich Center for the Economics of Aging, Max Planck Institute for Social Law and Social Policy, 80799 Munich, Germany

Edited by Marcus E. Raichle, Washington University in St. Louis, St. Louis, MO, and approved March 23, 2021 (received for review October 29, 2020)

The finding of reduced functional MRI (fMRI) activity in the default mode network (DMN) during externally focused cognitive control has been highly influential to our understanding of human brain function. However, these negative fMRI responses, measured as relative decreases in the blood-oxygenation-level–dependent (BOLD) response between rest and task, have also prompted major questions of interpretation. Using hybrid functional positron emission tomography (PET)-MRI, this study shows that task-positive and -negative BOLD responses do not reflect antagonistic patterns of synaptic metabolism. Task-positive BOLD responses in attention and control networks were accompanied by concomitant increases in glucose metabolism during cognitive control, but metabolism in widespread DMN remained high during rest and task despite negative BOLD responses. Dissociations between glucose metabolism and the BOLD response specific to the DMN reveal functional heterogeneity in this network and demonstrate that negative BOLD responses during cognitive control should not be interpreted to reflect relative increases in metabolic activity during rest. Rather, neurovascular coupling underlying BOLD response patterns during rest and task in DMN appears fundamentally different from BOLD responses in other association networks during cognitive control.

PET-fMRI | FDG | working memory | default mode network | neurovascular coupling

More than 20 y ago, Shulman and colleagues described a set of brain regions that consistently showed low levels of functional brain activity during cognitive control tasks relative to a passive resting state (1). In their seminal paper, they reported data from nine [^{15}O]-positron emission tomography (PET) experiments with passive or low-level baseline conditions as well as active task conditions including either language or nonlanguage cognitive tasks. By subtracting baseline scans from active task scans they were able to identify areas displaying decreased blood-flow during the active task conditions, later conceptualized as a resting or "default" state of brain function (2, 3).

Since its early description as task-related decreases in PET-based measures of blood flow and oxygen consumption, activity in the default mode network (DMN) has been explored extensively using functional MRI (fMRI), and its function remains a topic of great interest in the cognitive neurosciences (4–6). fMRI work showed that an antagonistic relationship between the task-negative DMN and task-positive association networks, including the dorsal attention network (DAN), is also evident in functional connectivity studies without task, suggesting that it is an intrinsic feature of functional brain network architecture (7, 8).

A dominant view posits that task-negative BOLD responses (NBR) in DMN reflect a relative increase of activity in the DMN during rest, related to its role in unconstrained, internally directed thought, including autobiographical thoughts, thinking about past and future, and mind wandering (9–13). Recent work has begun to emphasize a more general role for the DMN in ongoing regulation and reconfiguration of brain dynamics and network states in varying contexts (4, 14–17) and also highlighted functional heterogeneity within the DMN (18, 19). On this view, decreased activity during task is reflective of such reconfigurations being more prominent during an unconstrained state. There is also substantial evidence that blood-oxygenation-level–dependent (BOLD) deactivations in the DMN during external cognitive control are relevant to understanding human cognition in disease. Individual differences in the strength of negative coupling between networks during cognitive control have been linked to task performance (20), and a failure to deactivate the DMN has been associated with increased attentional lapses (21), reduced task-performance in aging (22–24), Alzheimer's disease (23, 25), and schizophrenia (26, 27).

Despite the large influence that the DMN deactivations described by Shulman and colleagues have had on subsequent research and our understanding of large-scale association networks in human cognition, the division of large-scale cortical association

Significance

A consistent finding from functional MRI (fMRI) of externally focused cognitive control is negative signal change in the brain's default mode network (DMN), but it is unknown whether this reflects an increase of synaptic activity during rest periods or active suppression during task. Using hybrid PET-MRI, we show that task-positive fMRI responses align with increasing glucose metabolism during cognitive control, but task-negative fMRI responses in DMN are not accompanied by corresponding decreases in metabolism. The results are incompatible with an interpretation of task-negative fMRI signal in DMN as a relative metabolic increase during a resting baseline condition. The present results open up avenues for understanding abnormal fMRI activity patterns in DMN in aging and psychiatric disease.

Author contributions: L.J.S. and A.R. designed research; L.J.S., F.G., V.P.L., K.R., J.A., and A.R. performed research; L.J.S., F.G., A.H., L.R., R.L., J.A., and A.R. analyzed data; L.J.S. and A.R. wrote the paper; and L.J.S., F.G., A.H., L.R., R.L., V.P.L., K.R., J.A., and A.R. contributed to the revision and approved the final submission.

Competing interest statement: R.L. received travel grants and/or conference speaker honoraria within the last 3 y from Bruker BioSpin MR, Heel, and support from Siemens Healthcare regarding clinical research using PET/MR. He is a shareholder of the start-up company BM Health GmbH since 2019.

This article is a PNAS Direct Submission.

See online for related content such as Commentaries.

[1]To whom correspondence may be addressed. Email: lars.stiernman@umu.se or anna.rieckmann@umu.se.

This article contains supporting information online at https://www.pnas.org/lookup/suppl/doi:10.1073/pnas.2021913118/-/DCSupplemental.

Published June 30, 2021.

networks into antagonistic task-positive and task-negative networks has almost exclusively been demonstrated with noninvasive imaging modalities that depend on neurovascular coupling (i.e., fMRI, [^{15}O]-PET, and arterial spin labeling), leaving it uncertain whether deactivations and activations during externally focused cognitive control tasks reflect antagonistic patterns of synaptic activity.

The current understanding of the neurovascular coupling underlying NBR during task and whether they follow the same principles as positive BOLD responses (PBR) is limited. Invasive recordings of neural activity in animals combined with BOLD imaging have studied the NBR primarily in early sensory-motor regions and hippocampus with conflicting results (28–32). The limited number of animal studies on DMN deactivations have also failed to show clear evidence that task NBR in DMN are reflective of relative decreases in neural activity during externally focused cognitive control (33–37). Moreover, while direct recordings can offer conclusive evidence regarding neural firing, they lack the ability to cover the whole brain at once and explore the interactions between large-scale distributed networks without a priori specification of regions of interest (ROI).

[^{18}F]fluorodeoxyglucose (FDG) PET offers a noninvasive imaging technique with whole-brain coverage at millimeter resolution that provides a measure of synaptic activity that is independent of neurovascular coupling. In resting-state FDG scans, the DMN can be identified as a network with high metabolic activity, particularly in the posterior cingulate cortex (PCC) and precuneus (2, 38, 39). In 1988, Fox et al. (40) laid the foundation for "task FDG." Using several back-to-back FDG and ^{15}O injections, with and without a checkerboard task, they could show that both the cerebral metabolic rate of glucose (CMR_{glc}) and cerebral blood flow (CBF) increased dramatically during transient neural activation of visual cortex, greatly exceeding the cerebral metabolic rate of oxygen ($CMRO_2$). Despite some uncertainty concerning the origin of the CBF/$CMRO_2$ mismatch, this and other work at the time provided an important rational for the BOLD contrast. Recently, FDG imaging has been advanced to show that transient changes in glucose metabolism can be measured dynamically in a single scan in human subjects (41, 42). This functional PET (fPET) method relies on a modification of the traditional bolus injection paradigm into a slow infusion protocol that delivers a constant plasma supply of FDG to the cell, such that a dynamic change in the slope of the time activity curve is proportional to the rate of CMR_{glc}. Using this method, transient metabolic changes over task blocks that are only a few minutes long have been detected in task-relevant regions during visual stimulation and hand movement as well as visuospatial reasoning (41–46), demonstrating marked spatial overlap with BOLD responses during the same task (46).

In the current study, we used simultaneous fPET-fMRI to study concurrent changes in blood oxygenation and glucose metabolism during alternating blocks of rest and a working memory (WM) task. This task elicits (Fig. 1*C*) robust PBR in core WM regions within the frontoparietal control network (FPN) and DAN and NBR in the DMN. The primary aim was to test the hypothesis that task-positive and task-negative BOLD changes during this externally focused cognitive control task are physiological opposites also in terms of glucose metabolism. The results inform us whether the NBR in DMN during externally focused cognitive control compared to rest should be interpreted as a relative reduction in synaptic activity.

Results

An overview of the task design is shown in Fig. 1*A*. Participants performed both tasks with high accuracy (WM manipulation, M = 92.97%, SD = 5.22; WM maintenance, M = 97.25%, SD = 3.00), but there was a significant difference in performance between

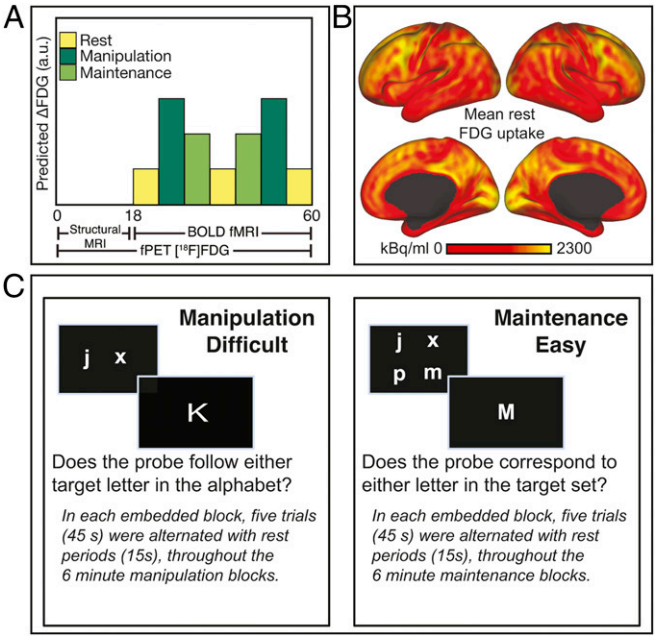

Fig. 1. Experimental setup. (*A*) Constant infusion of FDG started at time 0 and continued for 60 min. The FDG uptake was modeled using the GLM with separate regressors for the manipulation (difficult) and maintenance (easy) WM tasks in the shape of ramp functions that increase by one during the respective 6-min task blocks (i.e., after the two manipulation blocks that regressor has ramped up to 12). Structural images were collected during the first 18 min, and fMRI-BOLD data were collected between 18 and 60 min. To provide suitable contrast for both fPET and BOLD, an embedded block design is used (45), in which each "slow" 6 min task block has six "fast" 1-min blocks embedded within, each involving a 45-s task and 15-s rest. (*B*) Mean uptake of FDG averaged across subjects over the first 24-min task-free period. (*C*) The manipulation and maintenance WM tasks.

conditions, reflecting the increase in task difficulty for the WM manipulation condition (t (22) = 4.02, $P < 0.001$).

The main results from the hybrid PET-fMRI analysis below were based on conventional general linear model (GLM) analyses contrasting the difficult WM manipulation condition to rest and to the easier WM maintenance condition for each modality. To aid the interpretation of the main results, kinetic modeling of fPET was performed on PET time-series data in fMRI-defined ROIs.

PBR and Increases in Glucose Metabolism Overlap in Control and Attention Networks during WM. To establish feasibility of acquiring concomitant dynamic changes in task fMRI and PET during WM, we first tested the hypothesis that PBR and FDG increases show a high degree of overlap in the core task-positive networks. Fig. 2*A* shows the patterns for fMRI and fPET by modality as well as their spatial overlap in Fig. 2*B*. Both modalities showed significant increases for manipulation > rest in canonical WM regions belonging to the FPN, including dorsolateral PFC, ventrolateral PFC, anterior cingulate cortex, and superior parietal lobule as well as the DAN, including precentral gyrus and intraparietal sulcus. Refer to *SI Appendix*, Table S1 for a complete list of peak loci for fMRI and fPET. Importantly, both modalities also demonstrated an increased response with an increase in task demand (manipulation > maintenance) across the task-positive networks (Fig. 2*A*, bottom row), in line with recent results from a visuospatial task (46). Across contrasts, this shows that changes in glucose metabolism parallel PBR in task-positive regions, providing important initial support for the feasibility of the method and current design.

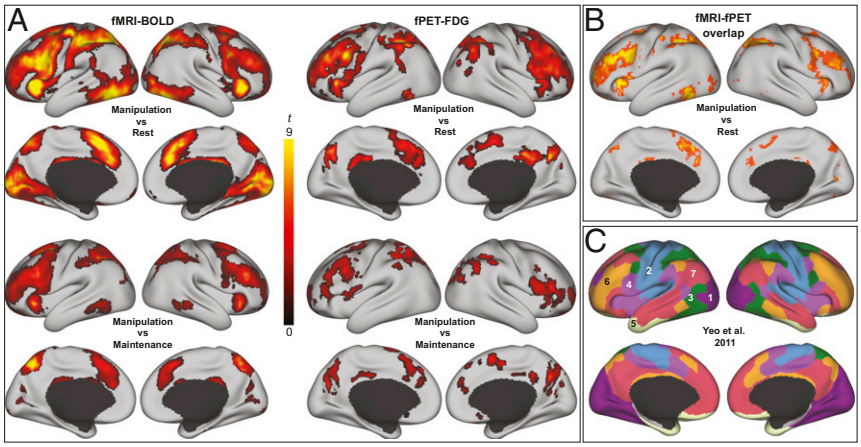

Fig. 2. Task-related increases in BOLD signal and glucose metabolism. (*A*) *t*-maps (corrected at $P < 0.05$) for fMRI (*Left*) and fPET (*Right*) were overlaid on an inflated surface in workbench view. Separate maps are shown for manipulation (the difficult WM condition) compared to rest (*Top*) and for the contrast manipulation > maintenance (*Bottom*). Both modalities showed significantly larger task-induced responses to manipulation compared to maintenance. (*B*) Overlap between fMRI and fPET at different uncorrected *t*-thresholds for the manipulation task ($P < 0.01$ to $P < 0.0001$, red to yellow, respectively) are modest in visual and sensorimotor networks at lower thresholds but high convergence in FPN and DAN also at more stringent thresholds. (*C*) The Yeo atlas (72) is displayed to provide a point of reference for the locations of task-related changes (1 = visual; 2 = sensorimotor; 3 = dorsal attention; 4 = ventral attention; 5 = limbic; 6 = frontoparietal; and 7 = default mode network).

Although largely overlapping increases for both modalities were observed in the FPN for manipulation > rest (Fig. 2*B* with reference parcellation in Fig. 2*C*), large BOLD signal changes in visual, motor, and sensorimotor cortices due to the sensory-motor demands of the task were not accompanied by FDG changes to the same extent; for FDG, task-related increases in visual cortex and left motor cortex were positive but nonsignificant at the a priori–selected, –corrected threshold.

The overlap map in Fig. 2*B* therefore shows the spatial overlap at different uncorrected thresholds, $P < 0.01$ (orange) to $P < 0.0001$ (yellow). In order to quantify the partial overlap between different functional networks and provide additional statistical support that voxels with FDG increases overlapped with those showing PBR primarily in FPN, DAN, and VAN, but also that FDG increases are more focal than the widespread PBR, overlap was computed separately for increases within a priori defined functional divisions in *SI Appendix*, Fig. S1 (*SI Appendix*, Table S1).

Task-Related NBR in the DMN Are Not Accompanied by Decreases in Glucose Metabolism. The next set of analyses explored whether a relative decrease in BOLD during task as compared to rest would also be paralleled by task-dependent decreases in FDG uptake. Because both modalities demonstrated the largest change for the contrast manipulation (difficult) > rest, the analyses in the following sections are based on the negative signal changes in this contrast, shown in blue in Fig. 3*A*, side by side for each modality (note that the patterns for maintenance > rest were similar but with overall weaker statistics). As expected, in fMRI, the DMN showed widespread NBR during manipulation as compared to rest, including PCC, medial prefrontal cortex (MPFC), inferior lateral parietal cortex, and lateral temporal cortex. However, aside from small clusters in temporal cortex and anterior MPFC (explored further in *SI Appendix*, Fig. S2), no significant negative changes in glucose metabolism were observed in core regions of the DMN, (posterior midline Fig. 3*B* ROI 5, MPFC Fig. 3*B*, ROI 6 and 7, and lateral parietal cortices). In addition, task-related increases in FDG signal during manipulation > rest overlapped with the DMN NBR in right posterior midline (Fig. 3*B* ROI 8). Interestingly, FDG increases were also observed in precuneus (Fig. 3*B* ROI 9) as well as left and right angular gyrus and anterior caudate even though BOLD signal changes were not significant in these regions.

Fig. 3*B* depicts the convergence of fMRI and PET in task-positive networks (ROIs 1 to 4) and the uncoupling of the two signals in DMN regions (ROIs 5 to 8) in bar graphs extracted from selected ROIs, highlighting the fact that lack of FDG signal changes in the DMN are not reflective of subthreshold FDG deactivation.

A number of control analyses were conducted in order to provide additional support for the conclusion that a NBR in DMN is not accompanied by task-related decreases in FDG. First, analyses of dice scores as a measure of overlap at different thresholds showed a striking lack of convergence of the two modalities in DMN, regardless of threshold (*SI Appendix*, Fig. S1*B*). In addition, *SI Appendix*, Fig. S2 shows a minimally thresholded image of FDG signal changes confirming that the observed lack of FDG decreases in core DMN regions along the midline was not merely due to a lack of power to detect negative change. Second, modeling the fMRI data in the same way as the PET data (i.e., as continuous 6-min task blocks) showed no notable differences in BOLD patterns of activation. This suggests that the differences in the underlying models that were due to the differing temporal resolution of each modality are unlikely to influence the ability to detect NBR in the DMN.

Finally, the absence of FDG signal decreases in response to the task in DMN was explored further with kinetic modeling of FDG data using standard PET compartmental modeling (47) in both simulations (*SI Appendix*, Fig. S3) and real data (Fig. 3*C*). Modeling of the observed data confirmed that FDG data in core regions of DMN NBR showed no notable change in k_3 throughout the experiment (Fig. 3*D*). Because our kinetic modeling is not dependent on an a priori–defined GLM, this shows that a lack of FDG change in regions of core DMN is not merely reflective of an ill-fitting a priori model. In contrast, PET modeling of the voxels showing increases showed that k_3 was highest during manipulation blocks, followed by maintenance, and lastly by rest. As suggested by high estimated k_3 throughout rest and task in DMN (and mean uptake prior to task, cf. Fig. 1*B*), we thus interpret the lack of task-related decreases in glucose metabolism in core DMN not as a relative absence of brain activity but as metabolic activity that remains high when individuals transition from rest to task.

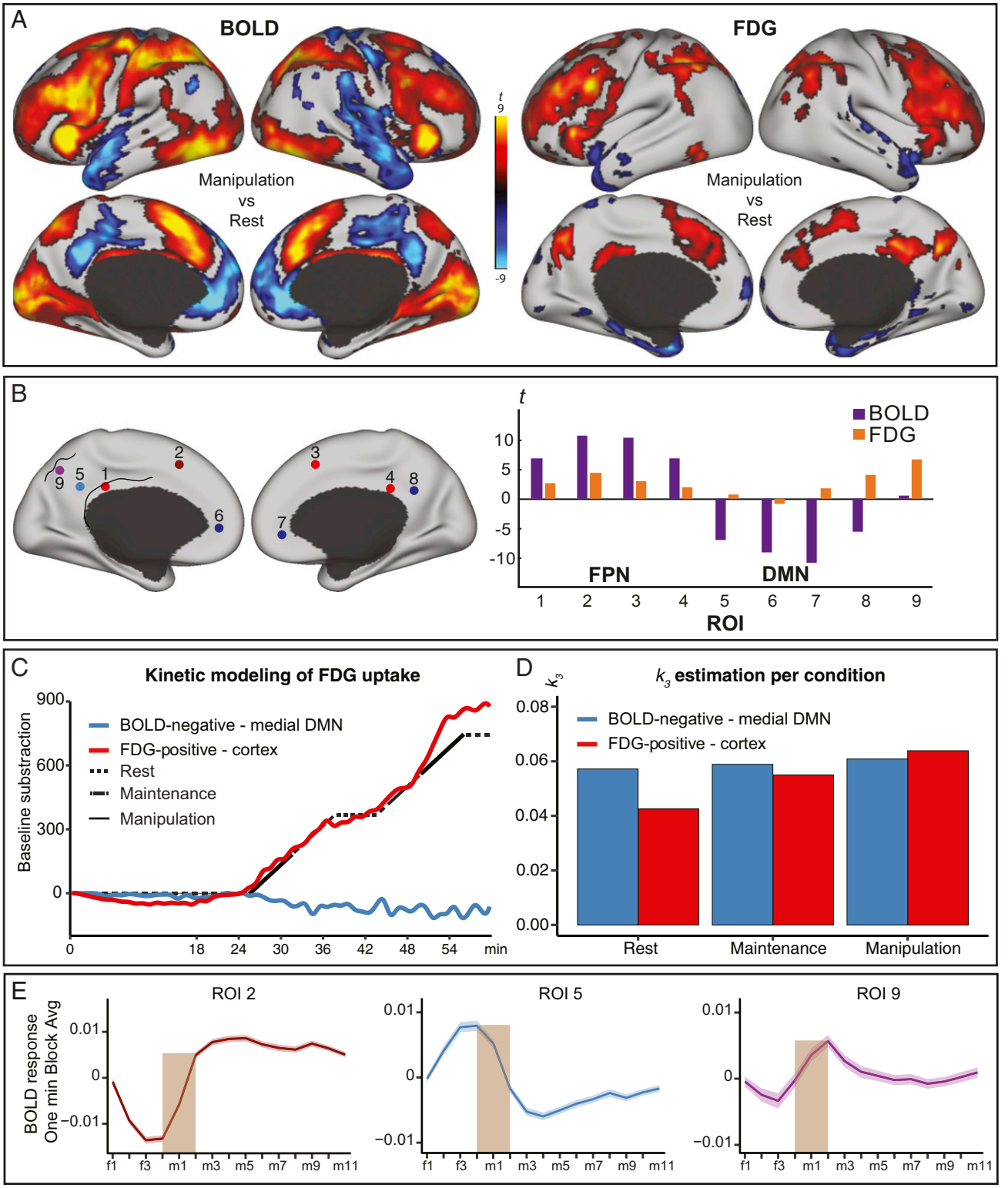

Fig. 3. Dissociation between the BOLD response and glucose metabolism in the posterior DMN. (*A*) *fMRI* and *PET* data for manipulation > rest in red and manipulation < rest in blue ($P < 0.05$, corrected). (*B*) *t*-statistics for BOLD (purple) and FDG (orange) at four loci selected from the BOLD analysis in the FPN (red), four from the DMN (blue), and one DMN loci selected from the fPET analysis in which there was no significant BOLD increase (purple). MNI coordinates were (1 [−6 29 27], 2 [−4 14 46], 3 [8 28 32], 4 [8 33 29], 5 [−8 50 29], 6 [−12 45 1], 7 [10 42 2], 8 [8 49 33], 9 [−2 −72 36]). (*C*) Kinetic modeling of the FDG signal was performed in two large ROIs reflecting FDG increases (red, manipulation > rest) (cf. *A*) and fMRI NBR in the DMN (blue, manipulation < rest in the medial frontal and posterior DMN). Residual FDG signal in the ROIs after subtracting the estimated baseline curve is represented by the red and blue lines. The black line illustrates the task structure. (*D*) The estimated k_3 for each condition and ROI are depicted with bars. (*E*) The BOLD signature in three ROIs, each representing a different multimodal pattern, are displayed for ROI 2, 5, and 9. The time-series of the 12 1-min embedded manipulation blocks were averaged across each of the four resting fixation TRs [f1 to f4] preceding each embedded task block, and the 11 TRs [m1 to m11] involving manipulation trials. The ribbon represents 1 SE. Of note, the time-series in 9 exhibits a transition-related response. DMN = default mode network, FPN = frontoparietal network, and ROI = region-of-interest.

The pattern of results observed in the cortex was largely similar in the striatum (*SI Appendix*, Fig. S4). With reference to a striatal parcellation by Choi and colleagues that allocated striatal voxels to their most strongly connected cortical network (48), both BOLD and FDG increased during manipulation in striatum-FPN, and striatum-sensorimotor displayed a significant PBR only. In striatum-DMN, only FDG increased without any change in BOLD.

In summary, while the PBR and FDG increases during WM align well in control and attention networks and to a lesser degree in sensory cortices, signal changes in the two modalities are uncoupled in the DMN. In DMN, fMRI shows a widespread NBR during task as compared to rest while FDG uptake remains comparably high, or displays increases, during the task.

One interesting exception to this general pattern were the regions of increased FDG signal without a concomitant change in BOLD signal, immediately adjacent to the DMN NBR. Thus, in a final set of analyses, we explored the BOLD signature that characterizes the posterior precuneus (Fig. 3 *B* and *E* ROI 9) in order to better understand whether the differences in fMRI and PET modeling alluded to above could account for this lack of convergence. As is evident from a visual comparison of BOLD signatures, the posterior precuneus is characterized by a sharp BOLD increase before the onset of each new task block followed by a signal that resembles the NBR in the rest of the DMN. This indicates that the region is, as suggested by the FDG increases, indeed involved in this task paradigm but is not captured accurately by the fMRI GLM because it shows features of both a PBR and NBR.

Discussion

In this study, we used simultaneous fPET-fMRI with a continuous infusion of FDG to assess whether changes in blood oxygenation in response to a WM task and rest are paralleled by changes in glucose metabolism across association networks. With FDG being a proxy for synaptic activity that is independent of blood flow, we reasoned that the results inform us whether NBRs during an externally focused cognitive control task are reflective of a relative decrease in synaptic activity in the DMN.

Increases in Blood Oxygenation and Glucose Metabolism Are Overlapping in Frontoparietal and Attention Networks. During performance of WM manipulation, compared to rest, overlapping increases throughout the FPN, and attention networks were detected for both modalities. Coupling between blood oxygenation and glucose metabolism aligns well with prior work in animals (28, 49) and humans (40, 50, 51) and conforms to the putative coupling between neural activity and BOLD signal. Of interest, despite robust and spatially extensive increases in BOLD, FDG signal increases were small and regionally focused in visual and motor areas. Because previous fPET studies have demonstrated metabolic increases in both visual and motor areas when these systems are explicitly taxed (41, 42, 44), we think this reflects the fact that the low demands on the primary visual cortex (letter versus fixation cross) and motor system (yes/no response during the probe) elicited only very small metabolic increases. These differences between different functional networks suggests that neurovascular coupling is not uniform across the cortex, as has been demonstrated for visual cortex and PCC in the macaque (35). A similar pattern was also observed in the striatum, with largely overlapping signals in the task-relevant associative striatum, but gradually decreasing PET signal toward posterior regions involved with sensory and motor processing.

Dissociations between Blood Oxygenation and Glucose Metabolism in Core DMN. The role of the DMN in human cognition remains a topic of wide interest. There is good evidence that the DMN is involved in internally focused mental operations when participants are instructed accordingly (e.g, refs. 12, 52, 53). What has remained a topic of debate is the interpretation of a relatively lower level of DMN activity during externally focused control tasks. The NBR may be reflective of an active suppression of irrelevant information processing when the environment demands externally focused attention or of a relative increase of this activity during the passive baseline condition (when individuals are instructed to rest and let their mind wander) (6). A third possibility is that NBR are reflective of a purely vascular change (i.e., vascular steal). In the current study, we found that robust and extensive NBR in distributed regions of the DMN were not paralleled by a relative decrease in glucose metabolism during task. The lack of a relative decrease in metabolism during task in the DMN is in stark contrast to the task-related changes observed in the task-positive areas, where the two modalities showed convergent increases during task. We argue that the observed uncoupling of blood oxygenation and glucose metabolism specific to DMN is not readily compatible with the latter two of the explanations that have been offered to account for the NBR above. First, the fact that the DMN is as metabolically active during rest as during cognitive control is difficult to reconcile with a notion that activity in the DMN is preferentially active during internally focused modes of cognition or, put bluntly, that rest is just another task state. Second, the kinetic model (Fig. 3*C*) and mean FDG uptake (Fig. 1) in DMN suggest that the lack of task-related decreases in DMN glucose metabolism in the current study reflects metabolic activity that remains high when transitioning between rest and task and not as an absence of activity. Accordingly, it is unlikely that task-related NBR are due to a purely vascular artifact (e.g., vascular steal). Hence, we are left to conclude that the NBR in DMN are reflective of a fundamentally different coupling between neural activity and blood oxygenation compared to PBR in task-relevant networks, possibly reflecting an active and energy demanding suppression of widespread DMN activity when association networks are engaged in external attention. In the next section, we discuss potential mechanisms that may guide future work to further explore this possibility.

A second important observation regarding the role of the DMN in human cognition is that glucose metabolism in DMN showed a heterogeneous pattern. For example, comparably high levels of glucose metabolism were observed in rest and task in MPFC and left posterior midline but significant increases in metabolism that overlapped with the NBR were apparent during task in right PCC (Fig. 3 *A* and *B*). Prior work has shown left PCC to be preferentially engaged in both episodic memory and mentalizing (theory of mind), whereas medial PFC and right posterior cingulate may be functional subsystems that are more specialized (19, 54). Why suppression of one of these subsystems would be more energetically demanding than another may have to do with the specific demands of the external attention and control task. Immediately adjacent to the NBR in DNM, a dissociation of BOLD and FDG responses was also observed in precuneus in which FDG showed robust increases during task but fMRI signal showed no signal changes. An exploration of the BOLD signal in this region revealed that the subthreshold fMRI signal was due to a task-related fMRI activation that was not captured by the GLM. Specifically, the BOLD time-series in posterior precuneus exhibited a task transition–related increase followed by a sustained response resembling the NBR in adjacent posterior cingulate. Activity related to a shift in context has been observed previously for regions belonging to the DMN in both humans (17, 55–57) and macaques (34, 35). Finally, we also observed heterogeneity of FDG signal changes within the areas of the NBR in MPFC, with a small cluster in frontal pole showing FDG decreases during task and aligning with BOLD here. Taken together, these patterns support the conclusion that there is high functional heterogeneity within the DMN (4, 14, 18, 58–60) that is not fully captured by task-related BOLD changes. The use of hybrid imaging that combines BOLD with a measure of synaptic activity may be able to identify functional heterogeneity also in the absence of explicitly taxing these subsystems.

Future work is needed to better link functional heterogeneity in synaptic activity to specific task demands across a range of different tasks, however.

In line with our current results, the limited number of animal studies or invasive human recordings have favored an interpretation of DMN NBR as a suppression of task-irrelevant activity (35, 36, 53, 61). Animal work has also highlighted the potential for altered neurovascular coupling underlying NBRs and that NBRs cannot be simply understood as "the opposite" of PBR (35). For example, despite reduced local field potentials across frequency bands in the cat PCC during a sensory discrimination task, an increase in neural firing was observed (33), counterintuitively suggesting that neural activity increases may result in task-negative responses during externally guided attention. Similarly, while there is evidence for suppression of gamma band activity in the macaque analog of PCC, concomitant increases in lower band frequencies have been observed during an attention task (36).

Neurovascular (Un)coupling across Networks. In order to provide plausible explanations for the dissociation between blood oxygenation and glucose metabolism in DMN, we next consider prior work that has investigated the physiological basis of human fMRI and PET signals. Based on the pioneering study of Fox et al. (40), joint increases in BOLD and FDG in core WM areas during the task likely reflect increased CMR_{glc}, coupled with increased $CMRO_2$ and a disproportionally large increase in CBF in response to increases in neural activity, especially in the gamma band (28). However, the current study suggests that these same mechanisms are not at play for NBRs during task because in the anterior DMN, but also parts of the posterior DMN, there is a relative decrease in the BOLD signal during task relative to rest, whereas FDG remains constant or increases. Following the same logic as in (1, 40) and studies linking FDG PET changes to CMR_{glc} (42), we take this pattern to reflect a relative decrease in CBF and/or $CMRO_2$ (62, 63) with constant or slightly increased CMR_{glc}. This suggests a different coupling between neural activity and vascular change in the DMN as compared to, for example, the FPN.

A recent study found similar to the present study, seemingly paradoxical results when comparing the effect of stimulation on the BOLD signal under various levels of baseline neural activity in the rat hippocampus (64). In that study, reduced BOLD signal could be explained by increases in $CMRO_2$. One potential explanation provided to explain the observed results was that the GABAergic system was activated in order to raise the threshold of activation for excitatory neurons to prevent seizures. This explanation could align with an active suppression account of DMN during task that is either equally demanding, or even more demanding, in terms of CMR_{glc} compared to freely resting. Thus, it appears plausible that while activations on control and attention networks are reflective of on-off changes in glutamatergic activity, eliciting known changes in CMR_{glc}, $CMRO_2$, and CBF, the GABAergic system may be specifically involved in the suppression of DMN activity during cognitive control and elicit metabolic demands on CMR_{glc} and $CMRO_2$ but with no "overshoot" of CBF. Indeed, optogenetic stimulation have identified different degrees of CBF for different GABAergic neuronal types (65). In order to gain a deeper understanding of what is causing the uncoupling between BOLD and FDG in the human DMN during WM, future research may for example combine pharmacological manipulations of the GABAergic system with fMRI and PET imaging during tasks. This may also provide further crucial information regarding the abnormal BOLD signal in the DMN observed in aging and neuropsychiatric disease (12).

Limitations. There are several limitations to this study. First, no arterial blood samples were collected, and absolute quantification of CMR_{glc} was therefore not possible. However, absolute quantification has been done to validate the GLM estimation of task-specific effects (42), and our k_3 estimation using the two-compartmental model aligned with the GLM results in both the FPN and DMN. Thus, the pattern of task changes in the absence of CMR_{glc} quantification would not affect the conclusions drawn in the current study. Moreover, we did not manipulate activity in response to a task that has previously been shown to increase BOLD signal as compared to rest in DMN (i.e., autobiographical thought). Thus, the conclusions from the current study remain specific to the comparison between rest and WM, and we cannot speak to metabolic changes in the DMN in response to other tasks that may further inform the cognitive operations rooted in the human DMN. Finally, the duration of task blocks may influence the appearance of metabolic decreases in DMN considering that decreases in anterior DMN were found for 10-min blocks, but not for block durations below 5 min in prior work (44). Nevertheless, the current timing and task design elicited robust changes in FDG that paralleled BOLD changes in task-positive networks, and there is no obvious reason why the design should conversely hinder the detection in the reverse contrast.

Conclusion

Using simultaneous FDG fPET and BOLD fMRI imaging during WM and rest, we show that fMRI PBR and NBR are not antagonistic in terms of synaptic activity. While BOLD and FDG signals align well in frontoparietal control and attention networks, only the BOLD signal showed a relative decrease in signal during the task in the DMN; glucose metabolism remained unchanged or increased during the task. The interpretation of DMN NBR as relative increases in neural activity during passive states, reflective of mind wandering or other forms of unconstrained thought, is not compatible with the current results. Rather, our results favor an explanation of DMN NBR as a reflection of active, energy-demanding suppression of task-irrelevant activity.

Materials and Methods

Participants. Participants were recruited via ads placed around the Umeå University campus and targeted healthy adults between 20 and 40 y of age with normal or corrected-to-normal vision. Exclusion criteria included history of head trauma, current or past diagnosis of a neurological or psychiatric illness, drug or alcohol abuse or dependence, and use of psychopharmaceuticals, drugs, or stimulants other than caffeine or nicotine for the past 6 mo. Individuals having an MRI-incompatible metallic implant or object in their body were excluded for MRI safety reasons. Pregnant or breast-feeding individuals, as well as persons having previously undergone PET scanning for research purposes, were excluded for radiation safety reasons. A total of 5 participants were excluded due to technical problems in the acquisition or poor data quality, resulting in a final sample size of 23 healthy young adults (mean age = 25.2, SD = 4.0, range = 20 to 37, 56.5% female) that entered the analyses for the current study. This study was approved by the Regional Ethics Committee at Umeå University.

Procedure. Participants were asked to fast for 4 h prior to scanning. Upon arrival, participants were informed about the study, signed the informed consent form, and then practiced the in-scanner task. After practice, blood glucose levels were measured to confirm that levels were below 7 mmol/l, and an intravenous needle used for infusion was placed in the left arm. Infusion of FDG diluted in saline started at time 0 of the PET-MR acquisition and continued for 60 min, distributing an initial radiation activity of ~180 MBq equally over the scan at a flow rate of 0.016 mL/sec. MRI sequences, starting from time 0, were in order: MRI attenuation correction, T1-weighted structural, T2-weighted fluid-attenuated inversion recovery (FLAIR), and, at the 18 min mark, fMRI continuously for 42 min. At the 60 min mark, a B0 sequence was performed to acquire field maps for fMRI bias field correction.

Verbal WM Task. Verbal WM was assessed during fMRI using two conditions of a letter-based task, each performed twice during scanning in blocks of 6 min each (i.e., 2 × 6 min maintenance and 2 × 6 min manipulation of letters in WM). Task blocks were interspersed with three 6-min rest blocks (Fig. 1*A*; task order: rest, manipulation, maintenance, rest, maintenance, manipulation,

rest). Within each of these 6-min task blocks, five WM trials (total 45 s) alternated with 15 s of resting fixation six times. Thus, within each "slow" 6-min task block were six 45-s "fast" blocks embedded. This design was chosen in order to accommodate the slow temporal resolution of PET but also be able to analyze fMRI data within slow blocks in terms of a traditional block design.

Whereas maintenance required only maintaining stimuli (letters) in WM, the manipulation condition also required the active transformation of stimuli in WM (*SI Appendix*). Robust fMRI responses to the task in canonical WM areas, FPN and DAN, have been reported in prior studies (66, 67). Prior to scanning, participants practiced four 1-min blocks in each condition to ensure they fully understood the tasks. No participant performed more than two practice runs.

PET/MRI Acquisition and Analysis. All imaging was performed on a 3T General Electric Signa PET-MR system with a 16-channel head coil. PET coincidence data were collected and reconstructed to 60 1-min frames using an OSEM (ordered-subsets maximization) algorithm with time-of-flight and point spread function modeling, two iterations, 28 subsets, and 6.4-mm post-filtering. Images were corrected for decay, scatter, and attenuation using an MR-based correction method (MRAC). The resulting voxel size was 0.97 × 0.97 × 2.81 mm3.

PET. After preprocessing (*SI Appendix*), task-related changes in the slope of the time-activity curve (TAC) were analyzed using the GLM approach described by refs. 41, 42. Prior to task analysis, simulations of the task paradigm using a two-compartment pharmacokinetic model of FDG (47, 68, described in detail below, were performed to establish that the model would reveal kinetically plausible k3 changes in response to our task design and the task contrasts task > rest (i.e., activations) and task < rest (i.e., deactivations; *SI Appendix*, Fig. S3). In addition to establishing feasibility of the task design, this exercise indicated that a task-induced change in k3 would influence the measured PET signal by only a small fraction during the first 2 min, because the increase in bound tracer is offset by a decrease of free tracer. In fact, a delay in the measurable change in FDG uptake in response to task onset can also be appreciated from the simulation figure in the original fPET publication (41) but was never discussed in their work. Thus, separately for each condition, task blocks were modeled as a ramp function with slope = 1 during the specific task and slope = 0 during rest and the other task. The task regressors were shifted forward by 2 min to account for the delay indicated by the simulations. A baseline regressor was defined by a third-order polynomial across all gray matter voxels with the task regressors modeled as nuisance variables. The task regressors were then orthogonalized to the baseline regressor and added to the final GLM along with six nuisance movement regressors (x, y, z, yaw, pitch, and roll). Finally, FDG task regressors were orthogonalized. However, considering that the manipulation task also requires maintenance of information in WM, if added first into the GLM, it may capture all common variance despite orthogonalization. Accordingly, for the maintenance condition, we present statistics from a GLM with maintenance added first and for the manipulation condition with manipulation added first. The resulting beta maps were normalized to Montreal Neurological Institute (MNI) space using the T1-to-MNI deformation field from the fMRI analysis pipeline. Higher-level analyses were performed using permutation testing with FMRIB Software Library (FSL) randomize (69) and 5,000 permutations. A threshold-free cluster-enhancement (TFCE) threshold of $P < 0.05$ identified significant voxels. The main effects of manipulation or maintenance > rest as well as the contrast manipulation > maintenance were the contrasts of interest.

Kinetic Modeling of Dynamic FDG Changes. While the GLM approach described above can identify relative changes in TAC slope as a function of condition, glucose metabolism cannot be quantified in an absolute sense without blood sampling. In order to address this potential shortcoming, we verified that the observed changes in task-induced FDG signal across association networks conformed to standard PET compartmental modeling (Fig. 3*C*) by quantifying k3 using the same FDG two-compartment pharmacokinetic model (47, 68) that we used in the simulations. The arterial input curve from ref. 41, which used the same dose of injected radiotracer as in the present study, was parametrized and used as the input curve. The first 24 min post injection was a period of rest, which fulfills the assumptions for this model. A reference TAC (all gray matter voxels) from this rest phase was fitted to the kinetic parameters K1, k2, k3, k4, fractional blood volume, and a blood-curve calibration factor to accommodate the unknown scaling of the parametrized blood-input. It was found that Vb did not change the quality of the fit, so it was excluded.

The fitted parameters K1, k2, k3, and k4 now define the rest-phase PET-uptake, f(t). This curve, extrapolated to the whole scan duration, represents the nonactivated uptake. The amplitude of f(t) may in practice be scaled by region-specific differences in tissue accessibility and, maybe more prominently, differences in partial-volume effects. Describing such differences by a multiplicative factor, s, the measured PET uptake in the rest-phase can be described as CROI,r = s · f(t). The factor s also relates the ROI 0 to 24 min area-under-the-curve for the rest-phase (AUCROI,r) to that of the reference region (AUCref,r), giving AUCROI,r = s · AUCref,r. Eliminating s from these two relations yields

$$C_{ROI,r}(t) = \frac{AUC_{ROI,r}}{AUC_{ref,r}} \cdot f(t) \quad [1]$$

and represents the nonactivated uptake-curve for the entire scan duration.

Baseline subtraction for a region was achieved by subtracting the time activity curve of the nonactivated curve (Eq. 1) from that for the region, CROI(t)

$$C_{activation} = C_{ROI}(t) - C_{ROI,r}(t). \quad [2]$$

This alternative model approach was finally used in Fig. 3 *C* and *D* to estimate the kinetics in task-positive and task-negative areas.

MRI.

T1-weighted. Structural T1-weighted images were acquired for 7.36 min with the following acquisition parameters: [field of view (FOV): 25 × 20, matrix: 256 × 256, Slice Thickness: 1 mm, Slices: 180, TE: 3.1 ms, TR: 7200 ms, Flip Angle: 12, and Bandwidth: 244.1 Hz/Pixel]. T1 images were used for tissue segmentation and normalization to standard MNI space using a preliminary 12 degrees of freedom (DOF) registration with FMRIB's Linear Image Registration Tool followed by a nonlinear registration using FMRIB's Nonlinear Image Registration Tool (70), resulting in 2-mm isotropic voxels.

fMRI. The BOLD data (Sequence parameters: FOV: 25.6, Matrix: 96 × 96, Slice Thickness: 3.6 mm, TE: 30 ms, TR: 4000 ms, Flip Angle: 80°, and Acceleration Factor: 2.0) were preprocessed following conventional steps for fMRI as implemented in FSL FMRI Expert Analysis Tool (FEAT) (https://fsl.fmrib.ox.ac.uk/) (70). Briefly, this included motion correction by volume-wise rigid body transformation to the first volume, slice timing correction, spatial smoothing (full-width half-maximum (FWHM) 5 mm), high-pass (120 s) temporal filtering, and correction for B0 inhomogeneities using a study-specific fieldmap template (*SI Appendix*). First-level statistics were obtained using the GLM. Manipulation and maintenance were modeled as separate regressors. Regressors of no interest were the extended motion parameters, frame-wise displacement (FD), white matter signal, and cerebrospinal fluid signal. All resting periods (showing a fixation cross), including those within the embedded blocks, were treated as an implicit baseline. (But refer to *SI Appendix*, Fig. S5 for a control analyses which excludes the embedded fixation periods.)

Matched with the PET model, the main effects of manipulation or maintenance > rest as well as the contrasts manipulation > maintenance and vice versa were the contrasts of interest. The resulting volumes were normalized to standard space using the T1-to-MNI deformation fields and a 6-DOF boundary-based registration between the first Echo Planar Imaging (EPI) volume and T1. Higher-level analyses were performed with FSL's randomise using 5,000 permutations and treating a TFCE threshold of $P < 0.05$ as significant for a given voxel. Post hoc exploration of signal changes were plotted in ROIs by placing a sphere with a radius of 5 mm (i.e., 5 voxels in diameter) at local peak effects.

Time-series analysis. In order to visually inspect and explore the BOLD signal in three ROIs, the BOLD time-series was extracted and averaged across participants. The following additional preprocessing steps were performed for the time-series analyses: normalization of time-series and application of a bandpass filter with the high-pass set to 180 s and lowpass to 6 s (i.e., half the block length and two-thirds the trial length). The ROIs were selected to illustrate the BOLD signal in three areas showing a different multimodal pattern along the left midline. For the manipulation > rest contrast, ROI 2 displayed increased BOLD and FDG, ROI 5 displayed a decrease in BOLD without a concomitant change in FDG, and ROI 9 displayed increased FDG but no change in BOLD. For illustration of condition-specific responses, the 12 "fast" embedded manipulation blocks within the longer manipulation blocks were averaged for each participant, each consisting of four TRs of passively observing a fixation cross (f1 to f4) and 11 TRs of performing the manipulation task (m1 to m11). To reduce influence of residual motion, TRs with a FD > 0.25 mm were excluded.

Data Availability. Code, processed imaging, and numerical source data that support the findings of this study are available at Open Science Framework (https://osf.io/yh48k) (71). The raw data from individuals are available from

NEUROSCIENCE

the Principal Investigator of the study on request, given appropriate ethical and data protection approvals.

ACKNOWLEDGMENTS. A.R. has received funding for this project from the European Research Council (ERC) under the European Union's Horizon 2020 research and innovation programme (ERC-STG-716065). L.R. is recipient of a DOC Fellowship of the Austrian Academy of Sciences at the Department of Psychiatry and Psychotherapy, Medical University of Vienna. The data collection was in part supported by financial contribution toward the Strategic Research Area Neuroscience (StratNeuro) at Umeå University. We thank the staff and leadership of Umeå Center for Functional Brain Imaging at Umeå University and Cancer Centrum and Nuclear Medicine at Umeå University Hospital for facilitating the data acquisition. For their contributions to data collection, analysis, or comments and discussions of preliminary results, we thank in particular Lars Nyberg, Helen Lindberg, Peter Young, Linda Douw, and Valentin Riedl.

1. G. L. Shulman *et al*., Common blood flow changes across visual tasks: II. Decreases in cerebral cortex. *J. Cogn. Neurosci.* **9**, 648–663 (1997).
2. D. A. Gusnard, M. E. Raichle, M. E. Raichle, Searching for a baseline: Functional imaging and the resting human brain. *Nat. Rev. Neurosci.* **2**, 685–694 (2001).
3. M. E. Raichle *et al*., A default mode of brain function. *Proc. Natl. Acad. Sci. U.S.A.* **98**, 676–682 (2001).
4. R. Leech, D. J. Sharp, The role of the posterior cingulate cortex in cognition and disease. *Brain* **137**, 12–32 (2014).
5. P. G. Spetsieris *et al*., Metabolic resting-state brain networks in health and disease. *Proc. Natl. Acad. Sci. U.S.A.* **112**, 2563–2568 (2015).
6. R. L. Buckner, L. M. DiNicola, The brain's default network: Updated anatomy, physiology and evolving insights. *Nat. Rev. Neurosci.* **20**, 593–608 (2019).
7. M. D. Fox *et al*., The human brain is intrinsically organized into dynamic, anticorrelated functional networks. *Proc. Natl. Acad. Sci. U.S.A.* **102**, 9673–9678 (2005).
8. P. Fransson, Spontaneous low-frequency BOLD signal fluctuations: An fMRI investigation of the resting-state default mode of brain function hypothesis. *Hum. Brain Mapp.* **26**, 15–29 (2005).
9. R. N. Spreng, R. A. Mar, A. S. N. Kim, The common neural basis of autobiographical memory, prospection, navigation, theory of mind, and the default mode: A quantitative meta-analysis. *J. Cogn. Neurosci.* **21**, 489–510 (2009).
10. R. L. Buckner, D. C. Carroll, Self-projection and the brain. *Trends Cogn. Sci.* **11**, 49–57 (2007).
11. R. N. Spreng, The fallacy of a "task-negative" network. *Front. Psychol.* **3**, 145 (2012).
12. R. L. Buckner, J. R. Andrews-Hanna, D. L. Schacter, The brain's default network: Anatomy, function, and relevance to disease. *Ann. N. Y. Acad. Sci.* **1124**, 1–38 (2008).
13. K. Christoff, Z. C. Irving, K. C. R. Fox, R. N. Spreng, J. R. Andrews-Hanna, Mind-wandering as spontaneous thought: A dynamic framework. *Nat. Rev. Neurosci.* **17**, 718–731 (2016).
14. F. M. Krienen, B. T. Yeo, R. L. Buckner, Reconfigurable task-dependent functional coupling modes cluster around a core functional architecture. *Philos. Trans. R. Soc. Lond. B Biol. Sci.* **369**, 20130526 (2014).
15. R. Leech, R. Braga, D. J. Sharp, Echoes of the brain within the posterior cingulate cortex. *J. Neurosci.* **32**, 215–222 (2012).
16. Z. Yang, R. C. Craddock, D. S. Margulies, C. G. Yan, M. P. Milham, Common intrinsic connectivity states among posteromedial cortex subdivisions: Insights from analysis of temporal dynamics. *Neuroimage* **93**, 124–137 (2014).
17. B. M. Crittenden, D. J. Mitchell, J. Duncan, Recruitment of the default mode network during a demanding act of executive control. *eLife* **4**, e06481 (2015).
18. R. M. Braga, R. L. Buckner, Parallel interdigitated distributed networks within the individual estimated by intrinsic functional connectivity. *Neuron* **95**, 457–471.e5 (2017).
19. R. M. Braga, K. R. A. Van Dijk, J. R. Polimeni, M. C. Eldaief, R. L. Buckner, Parallel distributed networks resolved at high resolution reveal close juxtaposition of distinct regions. *J. Neurophysiol.* **121**, 1513–1534 (2019).
20. A. M. C. Kelly, L. Q. Uddin, B. B. Biswal, F. X. Castellanos, M. P. Milham, Competition between functional brain networks mediates behavioral variability. *Neuroimage* **39**, 527–537 (2008).
21. D. H. Weissman, K. C. Roberts, K. M. Visscher, M. G. Woldorff, The neural bases of momentary lapses in attention. *Nat. Neurosci.* **9**, 971–978 (2006).
22. C. L. Grady *et al*., A multivariate analysis of age-related differences in default mode and task-positive networks across multiple cognitive domains. *Cereb. Cortex* **20**, 1432–1447 (2010).
23. C. Lustig *et al*., Functional deactivations : Change with age and dementia of the Alzheimer type. *Proc. Natl. Acad. Sci. U.S.A.* **100**, 14504–14509 (2003).
24. J. Persson, C. Lustig, J. K. Nelson, P. A. Reuter-Lorenz, Age differences in deactivation: A link to cognitive control? *J. Cogn. Neurosci.* **19**, 1021–1032 (2007).
25. M. D. Greicius, G. Srivastava, A. L. Reiss, V. Menon, Default-mode network activity distinguishes Alzheimer ' s disease from healthy aging: Evidence from functional MRI. *Proc. Natl. Acad. Sci. U.S.A.* **101**, 4637–4642 (2004).
26. M. L. Hu *et al*., A review of the functional and anatomical default mode network in schizophrenia. *Neurosci. Bull.* **33**, 73–84 (2017).
27. S. Whitfield-Gabrieli *et al*., Hyperactivity and hyperconnectivity of the default network in schizophrenia and in first-degree relatives of persons with schizophrenia. *Proc. Natl. Acad. Sci. U.S.A.* **106**, 1279–1284 (2009).
28. N. K. Logothetis, J. Pauls, M. Augath, T. Trinath, A. Oeltermann, Neurophysiological investigation of the basis of the fMRI signal. *Nature* **412**, 150–157 (2001).
29. K. J. Mullinger, S. D. Mayhew, A. P. Bagshaw, R. Bowtell, S. T. Francis, Evidence that the negative BOLD response is neuronal in origin: A simultaneous EEG-BOLD-CBF study in humans. *Neuroimage* **94**, 263–274 (2014).
30. A. Shmuel, M. Augath, A. Oeltermann, N. K. Logothetis, Negative functional MRI response correlates with decreases in neuronal activity in monkey visual area V1. *Nat. Neurosci.* **9**, 569–577 (2006).
31. N. Harel, S.-P. Lee, T. Nagaoka, D.-S. Kim, S.-G. Kim, Origin of negative blood oxygenation level-dependent fMRI signals. *J. Cereb. Blood Flow Metab.* **22**, 908–917 (2002).
32. U. Schridde *et al*., Negative BOLD with large increases in neuronal activity. *Cereb. Cortex* **18**, 1814–1827 (2008).
33. D. Popa, A. T. Popescu, D. Paré, Contrasting activity profile of two distributed cortical networks as a function of attentional demands. *J. Neurosci.* **29**, 1191–1201 (2009).
34. J. T. Arsenault, N. Caspari, R. Vandenberghe, W. Vanduffel, Attention shifts recruit the monkey default ode network. *J. Neurosci.* **38**, 1202–1217 (2018).
35. W. J. Bentley, J. M. Li, A. Z. Snyder, M. E. Raichle, L. H. Snyder, Oxygen level and LFP in task-positive and task-negative areas: Bridging BOLD fMRI and electrophysiology. *Cereb. Cortex* **26**, 346–357 (2016).
36. B. Y. Hayden, D. V. Smith, M. L. Platt, Electrophysiological correlates of default-mode processing in macaque posterior cingulate cortex. *Proc. Natl. Acad. Sci. U.S.A.* **106**, 5948–5953 (2009).
37. T. Kojima *et al*., Default mode of brain activity demonstrated by positron emission tomography imaging in awake monkeys: Higher rest-related than working memory-related activity in medial cortical areas. *J. Neurosci.* **29**, 14463–14471 (2009).
38. S. Minoshima *et al*., Metabolic reduction in the posterior cingulate cortex in very early Alzheimer's disease. *Ann. Neurol.* **42**, 85–94 (1997).
39. B. A. Vogt, L. Vogt, S. Laureys, Cytology and functionally correlated circuits of human posterior cingulate areas. *Neuroimage* **29**, 452–466 (2006).
40. P. T. Fox, M. E. Raichle, M. A. Mintun, C. Dence, Nonoxidative glucose consumption during focal physiologic neural activity. *Science* **241**, 462–464 (1988).
41. M. Villien *et al*., Dynamic functional imaging of brain glucose utilization using fPET-FDG. *Neuroimage* **100**, 192–199 (2014).
42. A. Hahn *et al*., Quantification of task-specific glucose metabolism with constant infusion of 18F-FDG. *J. Nucl. Med.* **57**, 1933–1940 (2016).
43. A. Hahn *et al*., Task-relevant brain networks identified with simultaneous PET/MR imaging of metabolism and connectivity. *Brain Struct. Funct.* **223**, 1369–1378 (2018).
44. L. Rischka *et al*., Reduced task durations in functional PET imaging with [^{18}F]FDG approaching that of functional MRI. *Neuroimage* **181**, 323–330 (2018).
45. S. D. Jamadar *et al*., Simultaneous task-based BOLD-fMRI and [18-F] FDG functional PET for measurement of neuronal metabolism in the human visual cortex. *Neuroimage* **189**, 258–266 (2019).
46. A. Hahn *et al*., Reconfiguration of functional brain networks and metabolic cost converge during task performance. *eLife* **9**, 1–18 (2020).
47. M. E. Phelps *et al*., Tomographic measurement of local cerebral glucose metabolic rate in humans with (F-18)2-fluoro-2-deoxy-D-glucose: Validation of method. *Ann. Neurol.* **6**, 371–388 (1979).
48. E. Y. Choi, B. T. T. Yeo, R. L. Buckner, The organization of the human striatum estimated by intrinsic functional connectivity. *J. Neurophysiol.* **108**, 2242–2263 (2012).
49. C. Magri, U. Schridde, Y. Murayama, S. Panzeri, N. K. Logothetis, The amplitude and timing of the BOLD signal reflects the relationship between local field potential power at different frequencies. *J. Neurosci.* **32**, 1395–1407 (2012).
50. Y. Nir *et al*., Coupling between neuronal firing rate, gamma LFP, and BOLD fMRI is related to interneuronal correlations. *Curr. Biol.* **17**, 1275–1285 (2007).
51. A. Kucyi *et al*., Intracranial electrophysiology reveals reproducible intrinsic functional connectivity within human brain networks. *J. Neurosci.* **38**, 4230–4242 (2018).
52. B. L. Foster, M. Dastjerdi, J. Parvizi, Neural populations in human posteromedial cortex display opposing responses during memory and numerical processing. *Proc. Natl. Acad. Sci. U.S.A.* **109**, 15514–15519 (2012).
53. K. C. R. Fox, B. L. Foster, A. Kucyi, A. L. Daitch, J. Parvizi, Intracranial electrophysiology of the human default network. *Trends Cogn. Sci.* **22**, 307–324 (2018).
54. J. R. Andrews-Hanna, R. Saxe, T. Yarkoni, Contributions of episodic retrieval and mentalizing to autobiographical thought: Evidence from functional neuroimaging, resting-state connectivity, and fMRI meta-analyses. *Neuroimage* **91**, 324–335 (2014).
55. V. Smith, D. J. Mitchell, J. Duncan, Role of the default mode network in cognitive transitions. *Cereb. Cortex* **28**, 3685–3696 (2018).
56. N. U. F. Dosenbach *et al*., A core system for the implementation of task sets. *Neuron* **50**, 799–812 (2006).
57. G. Arana-Oiarbide, R. E. Daws, R. Lorenz, I. R. Violante, A. Hampshire, Preferential activation of the posterior default-mode network with sequentially predictable task switches. *bioRxiv* [Preprint] (2020). https://doi.org/10.1101/2020.07.29.223180 (Accessed 21 January 2021).
58. D. S. Margulies *et al*., Situating the default-mode network along a principal gradient of macroscale cortical organization. *Proc. Natl. Acad. Sci. U.S.A.* **113**, 12574–12579 (2016).
59. J. M. Kernbach *et al*., Subspecialization within default mode nodes characterized in 10,000 UK biobank participants. *Proc. Natl. Acad. Sci. U.S.A.* **115**, 12295–12300 (2018).
60. M. P. van den Heuvel, O. Sporns, Network hubs in the human brain. *Trends Cogn. Sci.* **17**, 683–696 (2013).

61. T. Ossandón *et al*., Transient suppression of broadband gamma power in the default-mode network is correlated with task complexity and subject performance. *J. Neurosci.* **31**, 14521–14530 (2011).
62. J. Goense, H. Merkle, N. K. Logothetis, High-resolution fMRI reveals laminar differences in neurovascular coupling between positive and negative BOLD responses. *Neuron* **76**, 629–639 (2012).
63. A. Shmuel *et al*., Sustained negative BOLD, blood flow and oxygen consumption response and its coupling to the positive response in the human brain. *Neuron* **36**, 1195–1210 (2002).
64. F. Angenstein, The role of ongoing neuronal activity for baseline and stimulus-induced BOLD signals in the rat hippocampus. *Neuroimage* **202**, 116082 (2019).
65. M. B. Krawchuk, C. F. Ruff, X. Yang, S. E. Ross, A. L. Vazquez, Optogenetic assessment of VIP, PV, SOM and NOS inhibitory neuron activity and cerebral blood flow regulation in mouse somato-sensory cortex. *J. Cereb. Blood Flow Metab.* **40**, 1427–1440 (2020).
66. L. Nyberg *et al*., Age-related and genetic modulation of frontal cortex efficiency. *J. Cogn. Neurosci.* **26**, 746–754 (2014).
67. A. Rieckmann, S. Pudas, L. Nyberg, Longitudinal changes in component processes of working memory. *eneuro* **4**, ENEURO.0052-17.2017 (2017).
68. L. Sokoloff *et al*., The [14C]deoxyglucose method for the measurement of local cerebral glucose utilization: theory, procedure, and normal values in the conscious and anesthetized albino rat. *J Neurochem.* **28**, 897–916, https://doi.org/10.1111/j.1471-4159.1977.tb10649.x (1977).
69. A. M. Winkler, G. R. Ridgway, M. A. Webster, S. M. Smith, T. E. Nichols, Permutation inference for the general linear model. *Neuroimage* **92**, 381–397, https://doi.org/10.1016/j.neuroimage.2014.01.060 (2014).
70. M. Jenkinson, C. F. Beckmann, T. E. J. Behrens, M. W. Woolrich, S. M. Smith, FSL. *Neuroimage* **62**, 782–790, https://doi.org/10.1016/j.neuroimage.2011.09.015 (2012).
71. L. J. Stiernman, SIMULTAN 2020. Open Science Framework. https://osf.io/yh48k/. Deposited 11 February 2021.
72. B. T. T. Yeo *et al*., The organization of the human cerebral cortex estimated by intrinsic functional connectivity. *J. Neurophysiol.* **106**, 1125–1165 (2011).